Design of two-dimensional polarization-selective diffractive optical elements with form-birefringent microstructures

Mark S. Mirotznik, David M. Pustai, Dennis W. Prather, and Joseph N. Mait

We describe a design methodology for synthesizing polarization-sensitive diffractive optical elements based on two-dimensional form-birefringent microstructures. Our technique yields a single binary element capable of producing independent phase transformations for horizontally and vertically polarized illumination. We designed two elements for operation at 10.6 μm and fabricated them in silicon. Qualitative experimental results agree with design predictions. © 2004 Optical Society of America

OCIS codes: 050.0050, 090.0090, 220.0220, 050.1380.

1. Introduction

Phase-only diffractive optical elements (DOEs) are an attractive technology for a variety of applications in photonics and optoelectronics where arbitrary wave-front generation is desired. The small size and ability of DOEs to generate complex wave fronts contributes to its popularity, particularly for applications involving monochromatic illumination. Most DOEs are designed by algorithms based on scalar diffraction theory and are fabricated with large features relative to the operational wavelength. Unfortunately, these characteristics render the DOE insensitive to polarization, which offers an additional degree of freedom in optical and photonic system design.[1] Exploiting the polarization enables applications such as polarimetric imaging[2,3] and polarization-based switching.[4]

Over the past decade several investigators, including us, have developed techniques for constructing polarization-selective DOEs.[4–14] These devices are capable of generating independent phase profiles for two orthogonal linear polarizations. To construct polarization-selective DOEs, investigators have used either two anisotropic substrates[5–7,12] or a single form-birefringent structure.[8–11,13] Devices fabricated with two anisotropic substrates, usually calcite[12] or lithium niobate,[5,7] are effective but challenging to fabricate and align. Fabrication of a form-birefringent microstructure from a single substrate is therefore an attractive alternative. Form birefringence permits a designer to engineer desired anisotropic properties of a DOE onto a single substrate. In addition to providing greater control of the phase profile than two anisotropic substrates, exploiting form birefringence simplifies fabrication to a single binary etch and eliminates misalignment between substrates. Moreover, since the substrate does not require natural birefringence, conventional materials can be employed, which allows mature fabrication processes to be used.

Previous investigators have commented that the major disadvantage of the form-birefringent method is that the requirement for subwavelength features limits the method to long wavelengths in the infrared. However, advances in modern lithography have largely removed this limitation. In fact, binary DOEs can be fabricated with feature sizes less than 0.1 μm, which implies that form-birefringent microstructures can be fabricated for operation at visible wavelengths.[10,11]

Xu *et al.*[7,8] were one of the first groups to apply form birefringence to the fabrication of a polarization-selective computer-generated hologram (CGH). They designed one-dimensional form-birefringent CGHs using the second-order effective-medium the-

M. S. Mirotznik (mirotznik@cua.edu) is with the Department of Electrical Engineering and Computer Science, Catholic University of America, 201 Pangborn Hall, Washington, D.C. 20064. D. M. Pustai and D. W. Prather are with the Department of Electrical and Computer Engineering, University of Delaware, 140 Evans Hall, Newark, Delaware 19716. J. N. Mait is with the U.S. Army Research Laboratories, AMSRD-ARL-SE-EM, 2800 Powder Mill Road, Adelphi, Maryland 20783.

Received 23 April 2004; revised manuscript received 14 August 2004; accepted 16 August 2004.

0003-6935/04/325947-08$15.00/0

ory. Yu *et al.*[10] and Mirotznik *et al.*[13] extended form-birefringent design to two-dimensional polarization-selective CGHs. However, the individual phase transformations were restricted to binary values. The procedure required the design of four subwavelength gratings to produce four pairs of (x, y)-phase polarization values, i.e., $(0,0)$, $(0,\pi)$, $(\pi,0)$, and (π,π). Both the effective-medium theory[15] and rigorous coupled-wave theory[16] have been used to determine these gratings. Given two arbitrary $(0,\pi)$ binary phase transmissions, the DOE is designed with a table look-up. Since the phase pair at each pixel location is realized by use of one of the four subwavelength gratings over an area, the encoding is referred to as cell oriented. In experiments, the method exhibited high polarization contrast.[10,13] The principal disadvantage of this method is its restriction to binary phase elements, which produces well-known Hermitian symmetric artifacts in the response and limits the maximum diffraction efficiency for a single polarization channel to approximately 40%.

In this paper we extend the cell-encoding procedure to synthesize two-dimensional polarization-selective DOEs that have nearly an arbitrary number of phase levels. The method eliminates the artifacts produced by binary phase elements and allows designers to produce more general polarization-selective DOEs. Several elements were fabricated and experimental results are provided as validation.

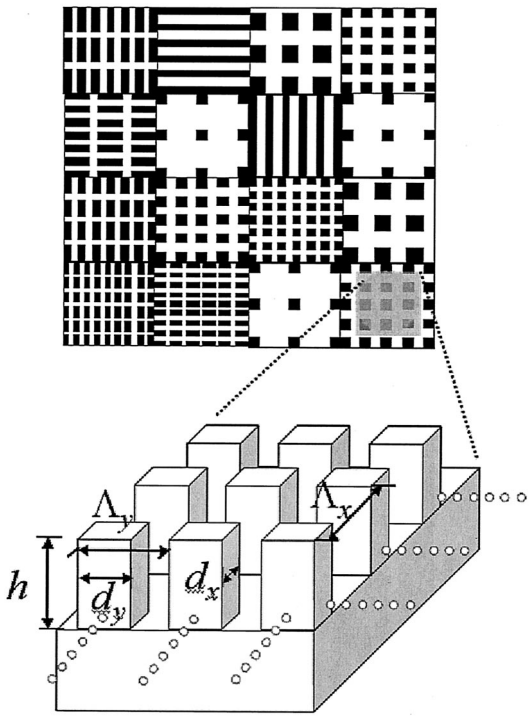

Fig. 1. Schematic representation of a form-birefringent DOE. A subwavelength grating at each pixel location produces polarization-dependent effective optical properties. Effective properties are a function of the x and y fill factors, the x and y grating periods, and the etch depth.

2. Design Methodology

A. General Concept

Phase-only DOEs are designed by means of mapping an optical phase function into a surface relief pattern. Typically, the phase function is realized by the modulation of the height of an area whose dimensions are fixed for each phase value. (This technique is referred to as point-oriented encoding.) If the dimensions of the diffracting feature are much larger than the illuminating wavelength, the phase transformation is insensitive to polarization.

To generate a DOE that is sensitive to polarization, its diffracting features must be less than or equal to the illuminating wavelength. Therefore, to generate a phase transformation that is sensitive to polarization, instead of height, the phase is encoded with subwavelength gratings. As represented in Fig. 1, the effective phase transformation is a function of the grating period, the fill factor, and the etch depth, as well as the bulk optical properties of the isotropic substrate. We note that, since the encoding is cell oriented, the phase can be encoded with grating parameters other than height. In fact, it is possible to fabricate a binary DOE that generates nearly an arbitrary number of phase levels. The grating will respond anisotropically if either the grating periods (Λ_x and Λ_y) or fill factors ($ff_x = d_x/\Lambda_x$ and $ff_y = d_y/\Lambda_y$) differ along the x and y directions. The grating period is given by Λ and the width of each binary feature within a single period by d.

Our design algorithm requires that we determine the phases ϕ^x and ϕ^y generated by varying the grating parameters d_x, d_y, Λ_x, and Λ_y. To do so, we used the rigorous eigenmode method described by Noponen and Turunen[16] to generate a look-up table of effective phases as a function of the grating's parameters. To ensure that each grating generates only a zeroth diffractive order in both transmission and reflection, we restrict the grating periods Λ_x and Λ_y to less than λ_0/n_s, where λ_0 is the free-space wavelength of illumination and n_s is the substrate index of refraction. Fabrication constraints will pose additional restrictions on the size of the minimum features and maximum aspect ratios that can be realized. Furthermore, to simplify fabrication, we restrict the grating to be binary and rectangular. In Subsection 2.B we briefly discuss our design procedure.

B. Effective Properties of Two-Dimensional Subwavelength Gratings

Two approaches have been primarily used to determine the effective optical properties of subwavelength gratings. With one approach, closed-form expressions[15,17] are used to provide approximate effective phase values as a function of the grating structure.[10] Although attractive from a computational perspective, the approximate expressions are accurate only for gratings whose period is much smaller than the wavelength of illumination. As the grating

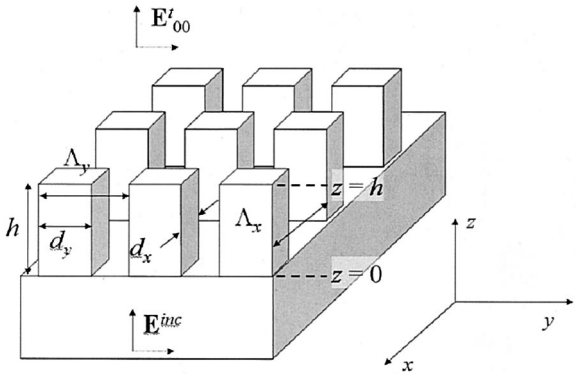

Fig. 2. Geometry used to calculate effective properties of subwavelength gratings.

period approaches the wavelength, which is referred to as the resonance regime, the assumptions on which these closed-form expressions are based are no longer valid.

We employ a second approach in which we utilize a rigorous electromagnetic model to determine the relationship between structural form and response. Although computationally more difficult, with this approach we are capable of generating accurate results for gratings of any period size. Several rigorous electromagnetic models can be used for this calculation; however, we believe that the rigorous coupled-wave algorithms offer the best compromise between accuracy and computational expense. To this end, we developed a rigorous model based on the method described by Noponen and Turunen[16] to calculate the effective optical properties of two-dimensional subwavelength gratings. The method is described briefly here. The reader is referred to Ref. 15 for a more detailed mathematical description.

The geometry of our structure, represented in Fig. 2, is a binary surface relief pattern sandwiched between two semi-infinite dielectric media. We denote the incident region as a semi-infinite space in which $z < 0$ and assume it consists of an isotropic dielectric of refractive index n_s. The illumination from the incident region is normally incident on the grating region defined by $0 < z < h$. Within the grating layer, the index of refraction is modulated between the substrate refractive index n_s and the transmission refractive index n_0. The transmission region is also a semi-infinite space in which $z > h$. We assume that this region is free space, $n_0 = 1$.

The incident field is a plane wave, linearly polarized in the x, y plane, and propagating in the $+z$ direction:

$$\mathbf{E}_{\text{inc}} = \hat{u} \exp(-jk_s z), \tag{1}$$

where $\hat{u}$ is a unit vector in the direction of propagation and k_s is the wave number of the incident region. The fields in the grating layer are described by the Floquet–Bloch theorem as a superposition of eigenmodes.[16] The diffracted fields outside the grating layer are expressed as a sum of diffracted orders of complex vector amplitudes $\mathbf{R}_{mn}$ for the incident region and $\mathbf{T}_{mn}$ for the transmitted region:

$$\mathbf{E}_R = \sum_{m,n} \mathbf{R}_{m,n} \exp[j(\alpha_m x + \beta_n y - r_{mn} z)],$$

$$\mathbf{E}_T = \sum_{m,n} \mathbf{T}_{m,n} \exp\{j[\alpha_m x + \beta_n y + t_{mn}(z - h)]\}. \tag{2}$$

The matching boundary conditions at $z = 0$ and $z = h$ produce a system of linear equations whose solution describes the field structure in all three regions. If the grating periods are constrained to be less than the material wavelength, i.e., Λ_x, $\Lambda_y < \lambda_0/n_s$, only the zeroth order, represented by $T_{0,0}$, propagates. Of primary interest to us is the relative phase lag introduced by the subwavelength grating:

$$\nabla\phi = \angle T_{0,0} - k_0 h, \tag{3}$$

where $\angle T_{0,0}$ denotes the angle of $T_{0,0}$ and k_0 is the free-space wave number.

One approach to cell encode a polarization-sensitive DOE is to evaluate Eqs. (2) and (3) at each pixel location. This requires the evaluation of numerous subwavelength grating structures to find one that best fits the design criteria. Consequently, Eqs. (2) need to be calculated thousands of times, which is clearly an impractical approach.

Instead, given a single substrate and a fixed etch depth, we generate a table of effective properties as a function of grating fill factors and periods. For example, Fig. 3 represents the relative phase and amplitude transmission of a subwavelength grating with etch depth $h = \lambda_0/(n_s - 1)$ corresponding to 2π phase and a substrate material with index of refraction $n_s = 3.4$ as the grating fill factor and grating period are varied. By restricting the periods and fill factors to only values that can be realized, we ensure that fabrication constraints are satisfied. Nonetheless, the results illustrate the relatively large phase discrimination one can achieve as the grating period increases from 50% to 90% of the wavelength in the material. Amplitude variations were found to be less than 15% for all fill factors and periods calculated in this study. We therefore employed a phase-only design strategy. We also note that, because the gratings lie within the resonance regime, we are unable to use the effective-medium theory to accurately calculate these effective properties.

The results shown in Fig. 3 are for an incident field linearly polarized in the y direction. By transposing the table, one obtains the phases for a field linearly polarized in the x direction. Thus only a single table of values is needed to generate all data required for design. The relationship between a single binary grating and the pair of phase values generated by two linearly polarized beams orthogonal to one another is represented in Fig. 4(a). As we describe in Subsection 2.C, it is the phase pairs generated by a single subwavelength grating that we use to design a form-birefringent cell-encoded DOE.

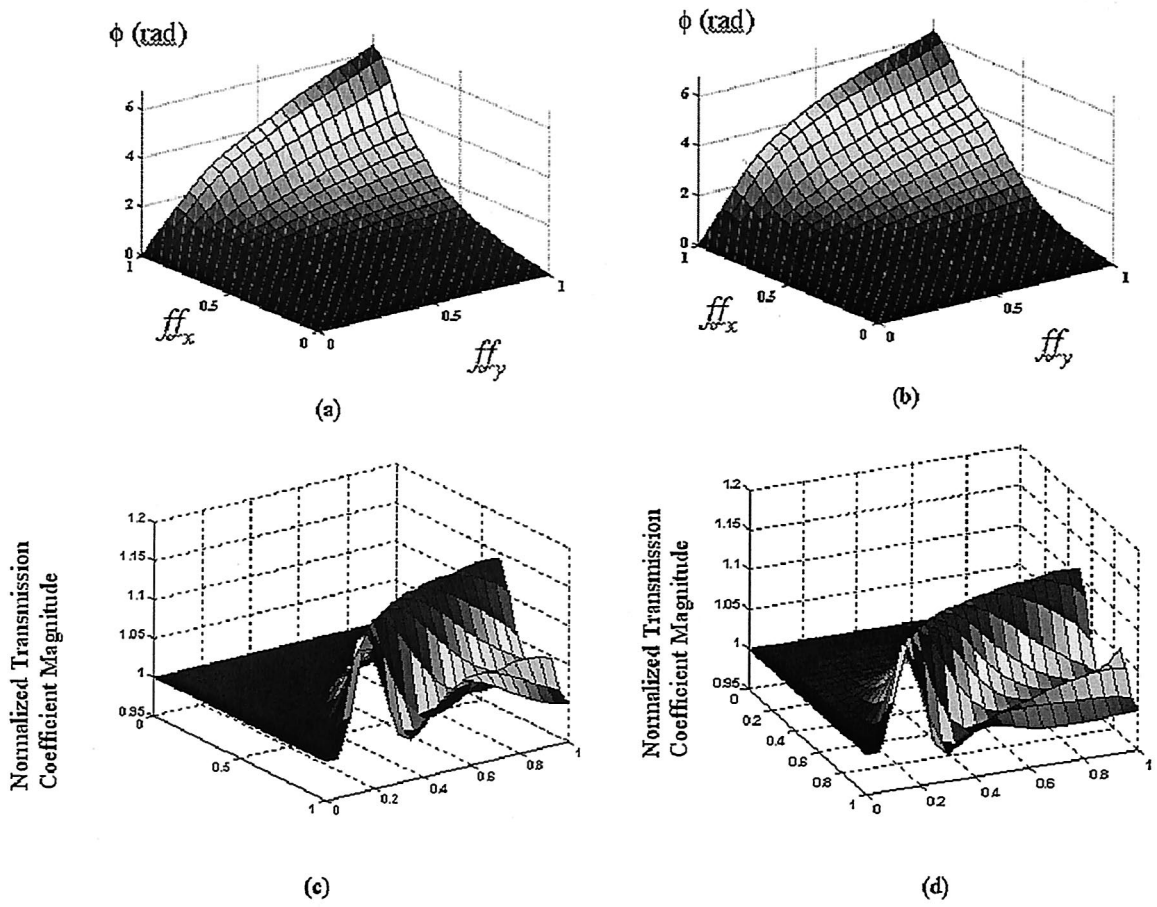

Fig. 3. Effective phase and amplitude transmission as a function of x and y fill factor. (a) Phase variations for $\Lambda_x = \Lambda_y = (0.5)\ \lambda_0/n_s$, (b) phase variations for $\Lambda_x = \Lambda_y = (0.9)\ \lambda_0/n_s$, (c) amplitude variations for $\Lambda_x = \Lambda_y = (0.5)\ \lambda_0/n_s$, (d) amplitude variations for $\Lambda_x = \Lambda_y = (0.9)\ \lambda_0/n_s$.

C. Design Algorithm

Given the effective media look-up tables, it is relatively straightforward to multiplex two independent continuous phase profiles with x- and y-polarized illumination. It is important, however, that the phase profiles are sampled on a scale larger than the wavelength. From trial and error we found that the phase profiles sampled as frequently as

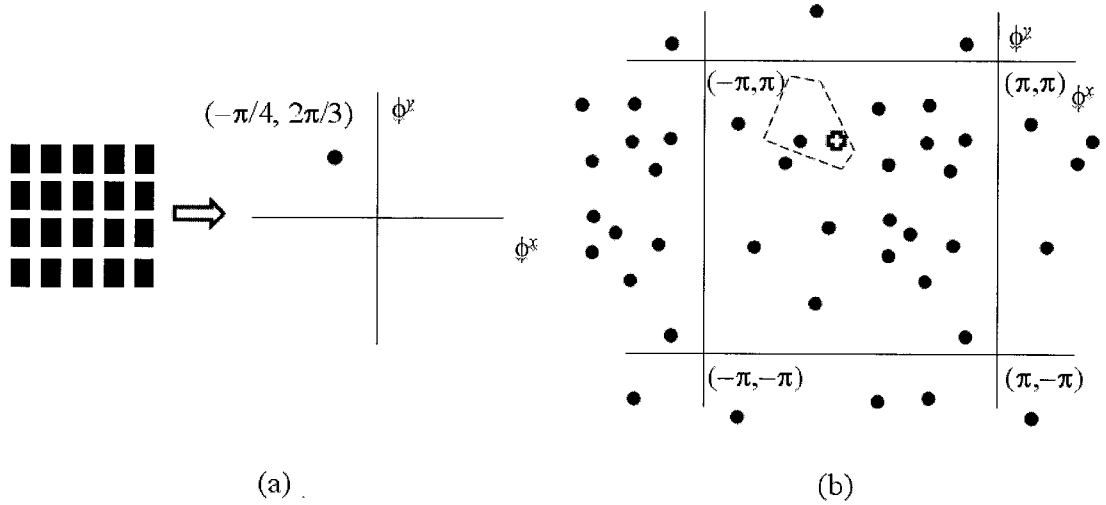

Fig. 4. Graphical representation of form-birefringent cell encoding. (a) Relationship between a single binary subwavelength grating and the pair of polarization-sensitive phase values. (b) The encoding of a desired phase pair by a subwavelength grating.

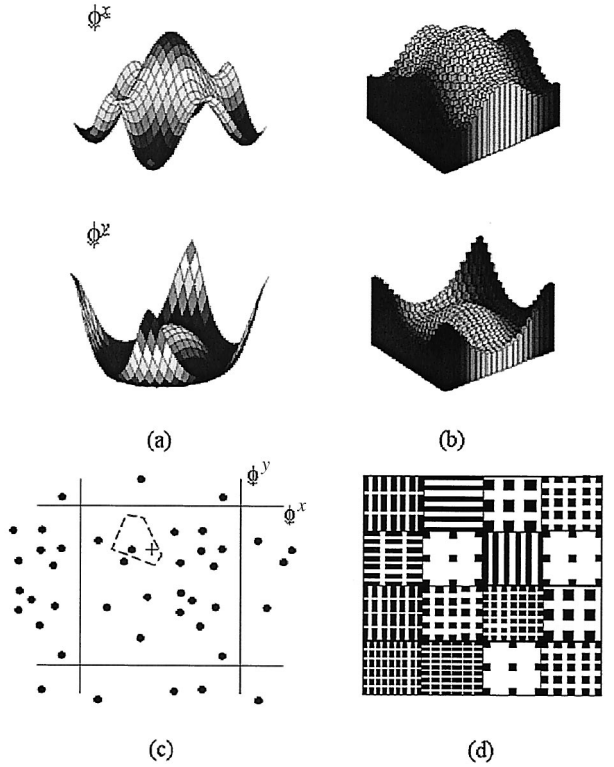

Fig. 5. Graphical representation of the algorithm used to design polarization-selective DOEs. (a) Desired phase profiles for x- and y-polarized illumination, (b) sampled phase profiles, (c) encoding, (d) binary cell-encoded polarization-sensitive DOE.

every five material wavelengths still produce good results. If the sampling distance is much smaller than this, the number of periods in the subwavelength grating is insufficient to generate the predicted effective optical properties. However, if the sample distance is too large, the superwavelength phase profiles do not adequately represent the desired transformation.

Given the desired independent phase values ϕ^x and ϕ^y for linear polarization along the x and y axes, respectively, at a single pixel, the pixel is encoded with the grating structure whose effective phase values are closest to the desired values. This is shown in Fig. 4(b), where all the phase pairs generated by the analysis of a discrete set of gratings are plotted in a two-dimensional space. Note that, due to the 2π periodicity in phase, the space is two-dimensionally periodic. Around one of the phase pairs, we indicate the region within which any desired phase pair is replaced by the associated grating structure. The boundary is determined when we minimize the error between the desired and the actual phase values:

$$\Delta\phi = [(\phi^x_{\text{desired}} - \phi^x_{\text{actual}})^2 + (\phi^y_{\text{desired}} - \phi^y_{\text{actual}})^2]^{1/2}. \quad (4)$$

The boundaries around the other points are not shown. The design algorithm is graphically illustrated in Fig. 5.

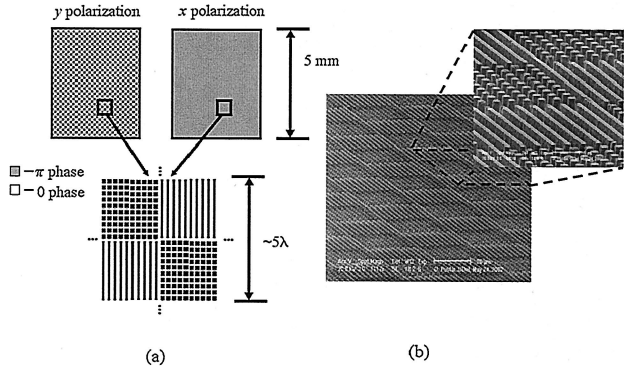

Fig. 6. Binary phase polarization-selective binary grating. (a) Desired phase profiles for x- and y-polarized illumination. (b) Scanning electron microscope image of the fabricated element.

3. Experimental Validation

To validate this method, we designed two polarization-selective DOEs using the method described in Section 2 for operation at $\lambda = 10.6$ μm. One element generated binary phase values for the two polarizations but the other generated a continuum of phase values from 0 to 2π. Both elements were fabricated by conventional lithography processes. First we spun a 750-nm-thick layer of polymethyl methacrylate (PMMA) onto a double-sided polished silicon wafer and then patterned the PMMA using electron-beam lithography. After development, the PMMA served as an etch mask to transfer the DOE pattern into the silicon by inductively coupled plasma reactive ion etching. By using a customized selective and anisotropic etch, we are capable of obtaining features as small as 50 nm with flat sidewalls and aspect ratios of the order of 10:1.

A. Binary Phase Polarization-Selective Binary Grating

We designed our first element such that y-polarized illumination is split into four beams of equal intensity but x-polarized illumination is undiffracted, i.e., the illumination responds to the element as though the element were a homogeneous dielectric slab. Thus y polarization must encounter a $(0,\pi)$ binary phase grating whereas x polarization senses only a constant phase. Given these conditions, we require only two grating structures, one to generate a (0,0) phase pair and the other to generate a $(0,\pi)$ phase pair.

The device, illustrated in Fig. 6(a), was designed in silicon ($n_s = 3.41$) for operation at 10.6 μm. At 4.7 μm, the etch depth corresponds to a phase delay slightly larger than 2π. The entire fabricated element, shown in Fig. 6(b), was 2.5 mm × 2.5 mm in size. Each unit cell was composed of ten subwavelength grating periods, approximately 25 μm × 25 μm in size, with a minimum feature size of 1.2 μm. Table 1 lists the desired and fabricated grating parameters used in this design example.

The experiment we used to characterize the element is represented schematically in Fig. 7. The source, a tunable CO_2 laser with a center wavelength of 10.6 μm, illuminates the DOE with linearly polar-

Table 1. Design Specifications for Binary Phase Polarization-Selective Binary Grating

Grating Phase Pair	h (μm)	ff		Λ (μm)		ϕ (rad)		$\Delta\phi$ (rad)
		ff_x	ff_y	Λ_x	Λ_y	ϕ^x	ϕ^y	
(0,π)								
Desired	4.7	0.40	1.00	2.5	2.5	1.07	4.22	3.15
Fabricated	4.6	0.43	1.00	2.4	2.4	1.16	4.26	3.10
(0,0)								
Desired	4.7	0.50	0.50	2.5	2.5	1.02	1.02	0.0
Fabricated	4.6	0.55	0.55	2.4	2.4	1.24	1.24	0.0

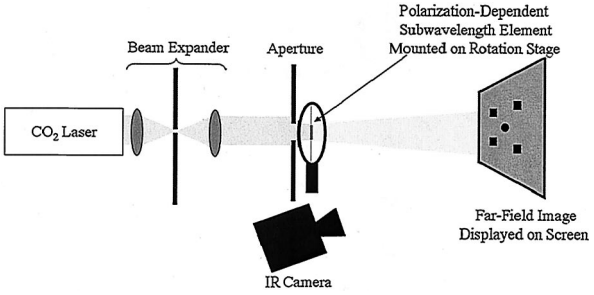

Fig. 7. Experimental setup used to characterize the polarization-selective DOEs.

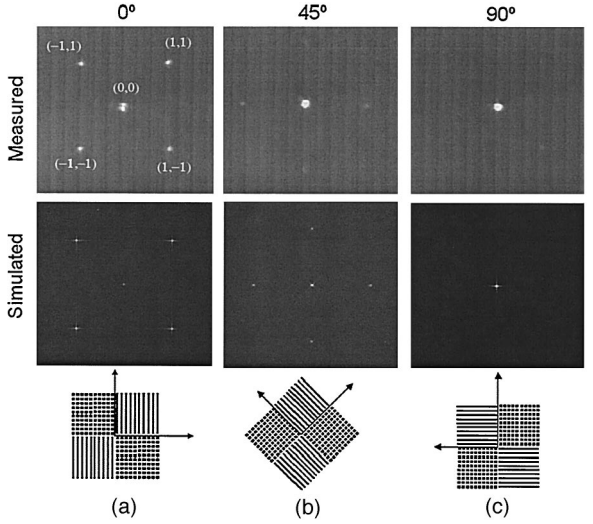

Fig. 8. Experimental results for the binary phase polarization-selective binary grating. Measured and simulated results for (a) x polarization, (b) linear polarization at 45°, (c) y polarization.

ized coherent radiation. The wave field diffracted by the DOE was imaged onto a viewing screen and digitally acquired with an IR camera and image grabber. We rotated the DOE about the optic axis to test its polarization-dependent behavior.

Simulated and experimental results, shown in Fig. 8, demonstrate the expected behavior of the device. For y-polarized illumination the zeroth and four first diffractive orders are clearly present. However, as the device is rotated the diffracted orders start to dim and, after rotation by 90°, i.e., when the polarization is in the orthogonal direction, only the zeroth diffractive order is visible. We conducted the simulations by propagating the complex field amplitudes within the object plane to the far-field using a Fourier transform. Both the experimental and the simulated results show the same qualitative behavior. However, the experimental results do reveal a much brighter on-axis spot than predicted. We believe this is primarily a consequence of light that was transmitted through the unetched portion of the sample. A more quantitative presentation of the results is given in Table 2. Here we determined the diffraction efficiencies by calculating the percent energy of each of the diffractive orders compared to the total amount of energy captured by the IR camera. As a comparative measure, the diffraction efficiencies of the simulated results are also provided. There is clearly a large discrepancy between the calculated and the measured results. We attribute the majority of this difference to the large on-axis spot in the measured results.

B. Multiple-Phase Polarization-Selective Blazed Binary Grating

We also designed a binary grating that corresponded to a linear blaze in the x direction for x-polarized illumination and a linear blaze in the y direction for y-polarized illumination. Figures 9(a) and 9(b) show the desired polarization-dependent phase responses. In this case the phase pairs range continuously between (0,0) and (2π, 2π). Fabrication parameters for this element were the same as for the first, except the minimum feature was 0.5 μm. The period of the blaze was 100 μm and the sampling distance was 10 μm. Thus each unit period was represented by a matrix of 10 × 10 phase pairs and subwavelength gratings. Given the 0.5-μm minimum feature, each subwavelength grating consisted of 20 × 20 features.

Table 2. Measured and Simulated Diffraction Efficiencies (in percent) for the Example Problem Described in Figs. 6 and 8

	Diffractive Order									
	(0,0)		(−1,−1)		(−1,+1)		(+1,−1)		(+1,+1)	
Diffraction Efficiency	y^a	x^b	y	x	y	x	y	x	y	x
Simulated	4.4	97.4	23.9	0.65	23.9	0.65	23.9	0.65	23.9	0.65
Measured	28.4	64.2	11.3	1.4	11.1	1.2	10.9	1.1	11.1	1.2

[a] y polarized.
[b] x polarized.

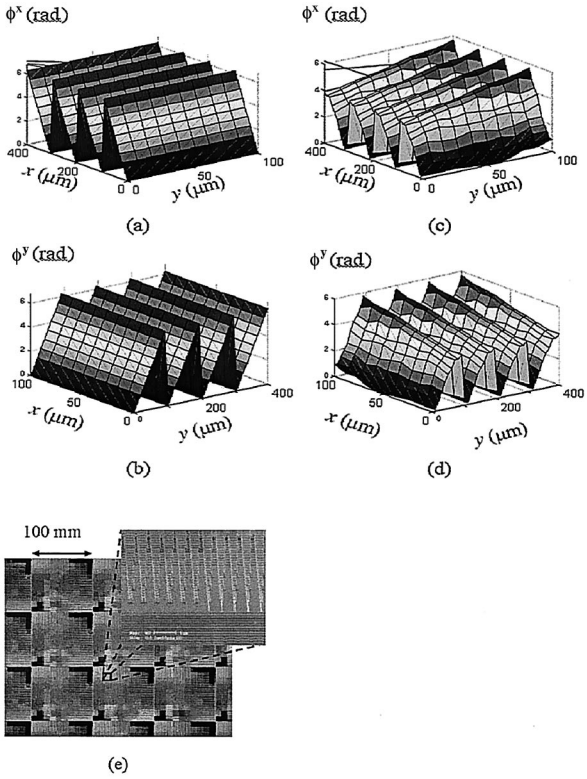

Fig. 9. Multiple-phase polarization-selective blazed binary grating. Desired phase profiles for (a) x- and (b) y-polarized illumination. Realizable phase profiles for (c) x- and (d) y-polarized illumination. (e) Images of the fabricated element.

The simulated phase responses generated by the encoded element are represented in Figs. 9(c) and 9(d). Substantial differences between the actual and the desired phase responses are clearly evident. In fact, at some locations the phase difference is as large as 35%. This is primarily due to our choice of a 500-nm minimum feature size. Although reducing the minimum feature below 0.5 μm allows us to design an element with a reduced phase error, the electron-beam write time required to fabricate such an element is prohibitively long. To fabricate a 3 mm × 3 mm element using 500 mm × 500 nm features took us 3.5 h to write all 6000 × 6000 individual features.

The fabricated element is shown in Fig. 9(e), and the results from our experimental characterization

Table 3. Measured and Simulated Diffraction Efficiencies (in percent) for the Example Problem Described in Figs. 9 and 10

	Diffractive Order									
	(0,0)		(−1,0)		(+1,0)		(0,−1)		(0,+1)	
Diffraction Efficiency	y^a	x^b	y	x	y	x	y	x	y	x
Simulated	5.4	5.2	5.1	0.8	62.0	6.8	5.3	5.4	0.9	61.0
Measured	33.4	31.6	6.1	2.4	28.2	3.3	4.1	4.3	2.9	27.9

[a] y polarization.
[b] x polarization.

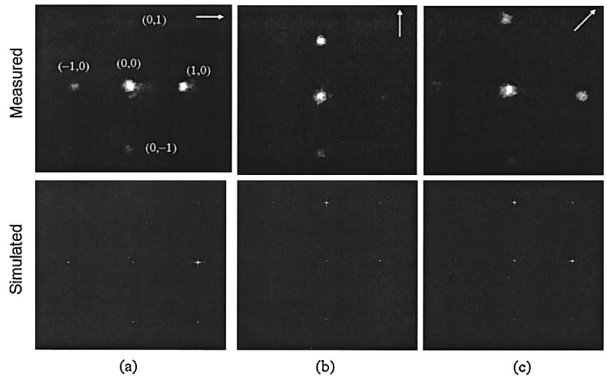

Fig. 10. Experimental results for the multiple-phase polarization-selective blazed binary grating. Measured and simulated results for (a) x polarization, (b) y polarization, (c) linear polarization at 45°.

are shown in Fig. 10 along with simulation results. The results for x polarization [Fig. 10(a)] clearly indicate the expected (+1,0) diffracted order. However, a bright on-axis spot and dimmer (−1,0), (0,−1), and (0,+1) diffracted orders are most likely a result of the phase errors that result from the encoding. We conducted the simulations by propagating the complex fields, calculated using the rigorous coupled-wave theory, to the far-field by a Fourier transform. Simulation results by use of the encoded phase responses, presented in Figs. 10(b) and 10(c), also reveal the presence of the on-axis and other diffractive orders seen during experiments. A more quantitative presentation of the results is given in Table 3. As in Table 2 we determined the diffraction efficiencies by calculating the percent energy of each of the diffractive orders compared to the total amount of energy captured by the IR camera. As in the previous example, the intense on-axis spot produced a large discrepancy between the measured and the simulated results.

4. Conclusion

In this paper we described a design methodology for synthesizing polarization-sensitive diffractive optical elements based on two-dimensional form-birefringent microstructures. Our technique yields a single substrate binary element that generates nearly independent phase responses for horizontally and vertically polarized illumination. In addition, we demonstrated how to use this method to synthesize polarization-selective binary DOEs that have a large number of phase levels in the phase response. Our technique simplifies the fabrication process and eliminates the artifacts produced by binary-phase elements. We presented experimental results for two elements operating at 10.6 μm that agreed with our predictions of expected polarization-dependent behavior. We are presently working to integrate our method into well-known CGH design algorithms to produce polarization-selective CGHs with multiple phase levels.

References

1. A. Lohmann, "Polarization and optical logic," Appl. Opt. **25,** 1594–1597 (1986).
2. D. Sabatke, M. Descour, and E. Dereniak, "Optimization of retardance for a complete Stokes polarimeter," Opt. Lett. **25,** 802–804 (2000).
3. G. P. Nordin, P. Deguzman, J. Jiang, and J. T. Meier, "Polarization sensitive diffractive optics for integration with infrared photodetector arrays," in *Diffractive Optics and Micro-Optics*, Postconference Digest, Vol. 41 of OSA Trends in Optics and Photonics Series (Optical Society of America, Washington, D.C., 2000), pp. 88–90.
4. A. Krishnamoorthy, V. Ashok, F. Xu, and J. Ford, "Polarization-controlled multistage switch based on polarization-selective computer-generated holograms," Appl. Opt. **36,** 997–1010 (1997).
5. N. Nieuborg, A. Kirk, B. Morlion, H. Thienpont, and I. Veretennicoff, "Polarization-selective diffractive optical elements with an index-matching gap material," Appl. Opt. **36,** 4681–4686 (1997).
6. L. Pajewski, R. Borghi, and G. Schettini, "Design of a binary grating with subwavelength features that acts as a polarizing beam splitter," Appl. Opt. **40,** 5898–5905 (2001).
7. F. Xu, J. Ford, and Y. Fainman, "Polarization-selective computer-generated holograms: design, fabrication, and applications," Appl. Opt. **34,** 256–266 (1995).
8. F. Xu, R. Tyan, P. Sun, Y. Fainman, C. Cheng, and A. Scherer, "Form-birefringent computer-generated holograms," Opt. Lett. **21,** 1513–1515 (1996).
9. J. Ford, F. Xu, K. Urquhart, and Y. Fainman, "Polarization-selective computer-generated holograms," Opt. Lett. **18,** 456–458 (1993).
10. W. Yu, T. Konishi, T. Hamamoto, H. Toyota, T. Yotsuya, and Y. Ichioka, "Polarization-multiplexed diffractive optical elements fabricated by subwavelength structures," Appl. Opt. **41,** 96–101 (2002).
11. S. Tao, X. Yuan, W. Cheong, J. Bu, and V. Kudryashov, "Optimized polarization-selective computer-generated hologram with fewer phase combinations," Opt. Exp. **11,** 1252–1257 (2003), http://www.opticsexpress.org.
12. N. Nieuborg, A. Kirk, B. Morlion, H. Thienpont, and I. Veretennicoff, "Highly polarization-selective diffractive optical elements in calcite with an index-matching gap material," in *Diffractive and Holographic Device Technologies and Applications IV*, I. Cindrich and S.-H. Lee, eds., SPIE Proc. **3010,** 124–133 (1997).
13. M. S. Mirotznik, J. N. Mait, and D. W. Prather, "Design of two-dimensional polarization selective computer generated holograms using form-birefringence," in *Diffractive Optics and Micro-Optics*, R. Magnusson, ed., Vol. 75 of OSA Trends in Optics and Photonics Series (Optical Society of America, Washington, D.C., 2002), pp. 231–233.
14. I. Richter, P. Sun, and F. Xu, "Design considerations of form-birefringent microstructures," Appl. Opt. **34,** 2421–2429 (1995).
15. P. Lalanne and J. Hugonin, "High-order effective-medium theory of subwavelength gratings in classical mounting: application to volume holograms," J. Opt. Soc. Am. A **15,** 1843–1851 (1998).
16. E. Noponen and J. Turunen, "Eigenmode method for electromagnetic synthesis of diffractive elements with three-dimensional profiles," J. Opt. Soc. Am. A **11,** 2494–2502 (1994).
17. M. Schmitz, R. Bräuer, and O. Bryngdahl, "Phase gratings with subwavelength structures," J. Opt. Soc. Am. A **12,** 2458–2462 (1995).